

SEARCH FOR MUON CATALYZED $d^3\text{He}$ FUSION

PNPI participants in the $^3\text{He}d\mu$ collaboration*):

V.A. Ganzha, K.A. Ivshin, P.V. Kravchenko, P.A. Kravtsov, E.M. Maev, A.A. Vasilyev, A.A. Vorobyov, N.I. Voropaev, M.E. Vmuzdaev

*) *Petersburg Nuclear Physics Institute, 188300, Gatchina, Russia;*

Paul Scherrer Institute (PSI), CH-5232 Villigen, Switzerland;

University of Washington, Seattle, WA, USA

University of Kentucky, Lexington, KY 40506 USA

Regis University, Denver, CO 80221 USA

1. Introduction

We report here on the results of an experiment aimed at observation of the muon catalyzed $d^3\text{He}$ fusion, which might occur after a negative muon stop in a $\text{D}_2 + ^3\text{He}$ gas mixture. The nuclear fusion reaction



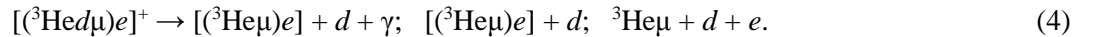
is interesting for various reasons: as a mirror reaction of the $d + t \rightarrow ^4\text{He} + n$ fusion process and as a perspective source of thermonuclear energy. This fusion process was involved in the primordial nucleosynthesis of light elements in the early Universe. For these reasons, it is important to know the cross section for this reaction at low collision energies $E < 10 \text{ keV}$. The phenomenon of muon catalysis of fusion reactions opens an opportunity to study this reaction at practically zero collision energy when fusion occurs in the $^3\text{He}d\mu$ mesomolecule:



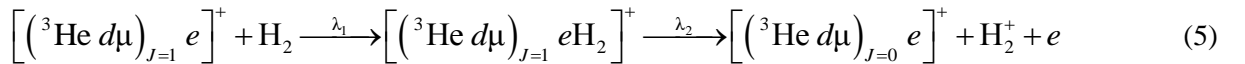
Formation of the $^3\text{He}d\mu$ molecule occurs in collisions of slow $d\mu$ atoms with ^3He atoms:



This process was first predicted by Y. Aristov *et al.* [1] in 1981 as an intermediate step in the muon transfer from the deuterium mesoatom to the helium atom. This prediction was confirmed in the experiments at PNPI, where the muon transfer rate was measured at room and at low temperatures: $\lambda_{d^3\text{He}}(300\text{K}) = (1.24 \pm 0.05) \cdot 10^8 \text{ s}^{-1}$, $\lambda_{d^3\text{He}}(50\text{K}) = (2.32 \pm 0.09) \cdot 10^8 \text{ s}^{-1}$, $\lambda_{d^3\text{He}}(39\text{K}) = (2.33 \pm 0.16) \cdot 10^8 \text{ s}^{-1}$, in close agreement with the predicted rates. The discovered formation process of the $^3\text{He}d\mu$ molecules allows to search for the muon catalyzed $d^3\text{He}$ fusion reaction, similar to the muon catalyzed dd and dt fusion reactions. However, a serious complication arises from competition of this fusion reaction with very fast decay of the $^3\text{He}d\mu$ molecule:



According to the theoretical calculations [2–4], the decay rate is $\lambda_{\text{dec}} \approx 7 \cdot 10^{11} \text{ s}^{-1}$. The nuclear fusion rates $\lambda_f(J)$ in the $^3\text{He}d\mu$ molecule depend strongly on the value of the molecular angular momentum J . The theoretical predictions are: $\lambda_f(J=0) \approx 2 \cdot 10^5 \text{ s}^{-1}$ and $\lambda_f(J=1) \approx 6.5 \cdot 10^2 \text{ s}^{-1}$ [5–6]. Unfortunately, about 99% of the initially produced $^3\text{He}d\mu$ molecules are in the $J=1$ state. However, as it was suggested by L. Menshikov and M. Faifman [7], the transition $(^3\text{He}d\mu)_{J=1} \rightarrow (^3\text{He}d\mu)_{J=0}$ is possible in collisions of the $[(^3\text{He}d\mu)e]^+$ complex with deuterium molecules *via* formation of a large molecular cluster $[(^3\text{He}d\mu)e\text{D}_2]$ and its decay:



with the formation and the transfer rates of this cluster $\lambda_1 \approx 3 \cdot 10^{13} \phi \text{ s}^{-1}$ and $\lambda_2 \approx 5 \cdot 10^{11} \text{ s}^{-1}$, respectively, where ϕ is the H_2 density normalized to the Liquid Hydrogen Density (LHD). Here H_2 stands for D_2 or HD . Such an estimate shows that one can expect quite efficient $(^3\text{He}d\mu)_{J=1} \rightarrow (^3\text{He}d\mu)_{J=0}$ transfer and, as a consequence, a detectable $^3\text{He}d\mu$ fusion process. The effective fusion rate λ_f can be defined as

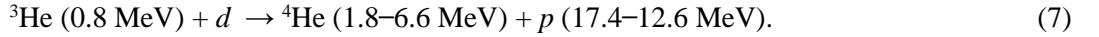
$$\lambda_f = P(J=0) \cdot \lambda_f(J=0) + P(J=1) \cdot \lambda_f(J=1), \quad (6)$$

where $P(J)$ is population of the ${}^3\text{He}d\mu$ molecule state with the angular momentum J . The population $P(J)$ is defined by the kinetics of formation, decay, transition and fusion in the ${}^3\text{He}d\mu$ molecule.

The first experimental limit on the effective muon catalyzed fusion rate $\lambda_f < 4 \cdot 10^8 \text{ s}^{-1}$ was set at PNPI in 1990 in an experiment with the $\text{D}_2 + {}^3\text{He}$ (5%) gas mixture. Next measurements were carried out in 1996 using the $\text{HD} + {}^3\text{He}$ (5.6%) gas mixture. During a short test run in the intense muon beam at PSI, the upper limit for the ${}^3\text{He}d\mu$ fusion rate was moved down to $\lambda_f < 1.6 \cdot 10^6 \text{ s}^{-1}$. Later in 1997, there was a special physics run at PSI aimed at observation of the muon catalyzed ${}^3\text{He}d$ fusion in the $\text{HD} + {}^3\text{He}$ (5.6%) gas mixture. This experiment resulted with a new upper limit for the effective fusion rate $\lambda_f < 6 \cdot 10^4 \text{ s}^{-1}$ [8].

On the other hand, another collaboration at PSI has undertaken in 1998 a search of the muon catalyzed ${}^3\text{He}d\mu$ fusion in the $\text{D}_2 + {}^3\text{He}$ (5%) gas mixture. The reanalysed results of that experiment were published in 2006 [9]. The authors declared the first observation of this process with the measured effective fusion rates: $\lambda_f = (4.5 + 2.6 / - 2.0) \cdot 10^5 \text{ s}^{-1}$ and $\lambda_f = (6.9 + 3.6 / - 3.0) \cdot 10^5 \text{ s}^{-1}$ at the D_2 density 5.21% and 16.8% of the LHD, correspondingly. Such a fusion rate exceeds by an order of magnitude the upper limit $\lambda_f < 6 \cdot 10^4 \text{ s}^{-1}$ set in our previous experiment. This striking difference might be related with problems of taking into account the background reactions, which could simulate the searched reaction (2). The main background of this type is due to the so-called ${}^3\text{He} + d$ fusion-in-flight. It comes from collisions with D_2 of the ${}^3\text{He}$ (0.8 MeV) nuclei produced in the $dd\mu$ fusion reaction. This background is more important in the $\text{D}_2 + {}^3\text{He}$ gas mixture than in the $\text{HD} + {}^3\text{He}$ gas mixture used in our experiment. On the other hand, the difference between the results of these two experiments might be also due to a possible difference in the formation and transfer rates λ_1 and λ_2 in the $[({}^3\text{He}d\mu)_{J=1} e\text{HD}]^+$ and $[({}^3\text{He}d\mu)_{J=1} e\text{D}_2]^+$ clusters.

Fortunately, the MuSun experiment, presently under way at PSI [10], gives us an excellent possibility to clarify the situation. The main goal of MuSun is to measure the muon capture rate in deuterium. For that, the lifetime of negative muons stopped in ultra clean D_2 gas is measured with high precision (10^{-5}). That requires very high statistics of the detected muon decays. In particular, $1.3 \cdot 10^{10}$ decays of the muons stopped in the sensitive volume of the MuSun active target were registered in Run 8 of this experiment. Besides muons, the active target detects also the products of the reactions initiated by muons, including the products of the ${}^3\text{He} + d$ fusion-in-flight :



Therefore, Run 8 can serve as a high statistical background experiment for an experiment aimed at searches of the muon catalyzed ${}^3\text{He}d\mu$ fusion in the $\text{D}_2 + {}^3\text{He}$ gas mixture.

Having this in mind, the decision was taken by the MuSun collaboration to perform an additional Run 9 with the active target filled with the $\text{D}_2 + {}^3\text{He}$ (5%) gas mixture, keeping all experimental conditions identical to those in Run 8. The results of these studies are presented below.

2. The MuSun experimental set-up

A principal scheme of the MuSun experiment is shown in Fig. 1. The incoming muons are detected first by a thin scintillator counter μSC and by a wire proportional chamber μPC . Then they pass through a 0.4 mm thick hemispheric beryllium window and stop in the sensitive volume of the time-projection chamber, TPC. The TPC is the key element of the experimental set-up. It is filled with ultra-pure protium-depleted deuterium gas at the temperature $T = 31 \text{ K}$ and pressure $P = 5 \text{ bar}$, and it operates as an active target in the ionization grid chamber mode (without gas amplification). Its main goal is to select the muon stops within the fiducial volume of the TPC well isolated from the chamber materials.

The trajectory and the arrival time of the muon decay electrons are measured with two cylindrical wire chambers $e\text{PC}1$, $e\text{PC}2$ and with a double layer scintillator hodoscope $e\text{SC}$ consisting of 32 plastic scintillators. The geometrical acceptance of the electron detector is 70%.

The ionization electrons produced in the TPC drift towards the anode plane in the electric field of 11 kV/cm with the velocity of 5 mm/ μs . The total drift space (the cathode – grid distance) is 72 mm. The anode plane is subdivided into 48 pads making a pad matrix of six pads (horizontal direction X) by eight pads (beam direction Z). The size of the pads is 17.5 mm (X) \times 15.25 mm (Z). About 50 % of the muons

passing through the μ SC are stopped within the fiducial volume above the 20 central pads at the distance of more than 1 cm from the cathode and from the grid (Fig. 2).

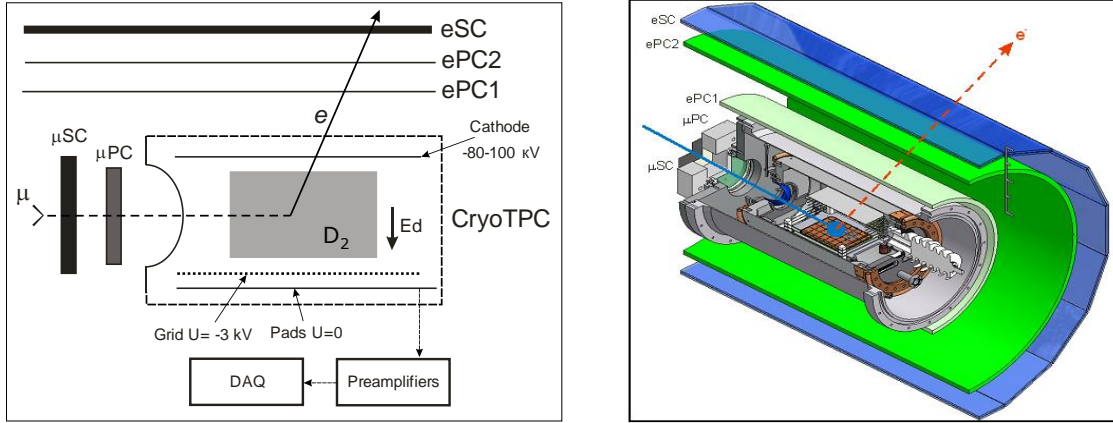


Fig. 1. Principal scheme of the MuSun experiment and schematic view of the MuSun set-up. The TPC is filled with ultra-pure protium-depleted deuterium gas at $T \approx 31$ K and $P \approx 5$ bar. The shadowed area shows a fiducial volume with muon stops far enough from all TPC materials

All anode pads have independent readout channels with fast (100 MHz) ADCs allowing to measure the amplitude, the duration, the energy, and the time of appearance of the signals with the amplitude exceeding the 80 keV threshold at any pad in the time window 0–25 μ s after a muon signal is detected by the μ SC counter. The same μ SC signal triggers the “muon-on-request” system, which switches off the muon beam thus excluding arrivals of other muons in the registration time window. The energy resolution (noise) in each channel is around 20 keV (sigma). The TPC measures the ionization produced by the entering TPC muon, determines its trajectory, and selects the 3D muon stop coordinate to be inside the fiducial volume isolated from all TPC materials. Also, the TPC detects products of reactions following the muon stop, including products of the ${}^3\text{He}d$ fusion.

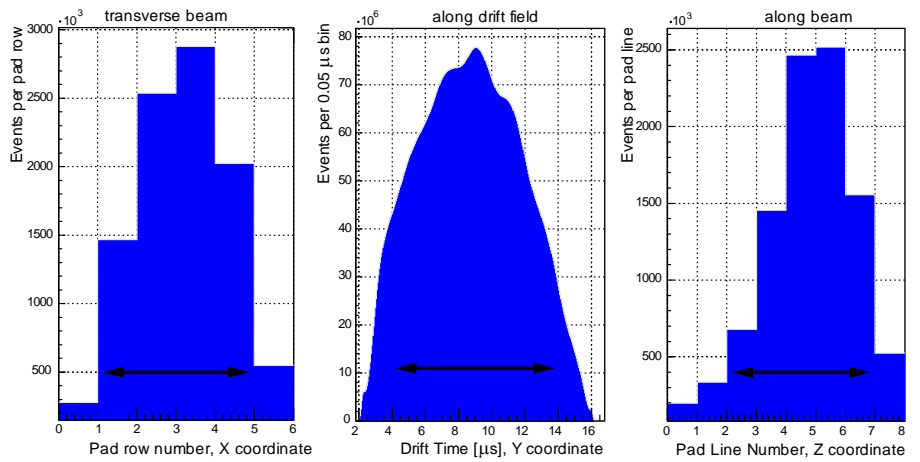


Fig. 2. The measured muon stop distribution inside the TPC sensitive volume. The double arrows show the fiducial volume selected in the present analysis

3. Experimental data and analysis

Table 1 compares the experimental conditions of the TPC in Run 8 and Run 9. The only difference is the gas filling. All other conditions are identical. In both runs, the ultra high gas purity was maintained by continuous operation of a gas purification system.

Table 1

Experimental conditions in Run 8 and in Run 9

Run	Gas filling	Temperature	Pressure	D ₂ density, C _d	Gas purity
Run 8	D ₂	31 K	5 bar	6.5% LHD	$< 2 \cdot 10^{-9}$ (N ₂)
Run 9	D ₂ + 5% ³ He	31 K	5 bar	6.2% LHD	$< 2 \cdot 10^{-9}$ (N ₂)

Figure 3 shows the scheme of processes initiated by a muon stop in the $D_2 + {}^3\text{He}$ gas mixture. For the goal of this experiment, it is important to know the yield of the ${}^3\text{He}d\mu$ molecules leading to possible muon catalyzed ${}^3\text{He}d$ fusion and the yield of the ${}^3\text{He}$ (0.82 MeV) nuclei responsible for the main background reaction: ${}^3\text{He} + d$ fusion-in-flight. Both yields can be precisely calculated, as the parameters entering the scheme in Fig. 3 are known with high accuracy [11]. On the other hand, the ${}^3\text{He}$ (0.82 MeV) yield can be determined directly from the experimental data as shown in Fig. 4.

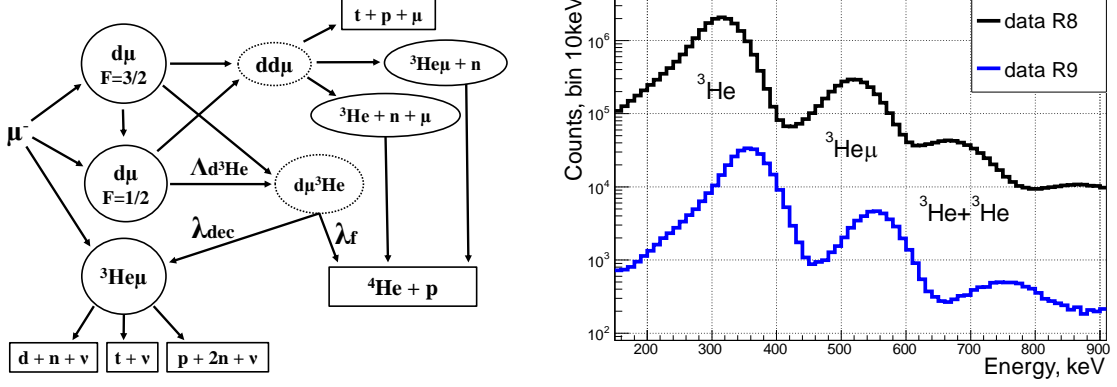


Fig. 3. Left panel: scheme of processes initiated by a muon stop in the $D_2 + {}^3\text{He}$ gas mixture. Right panel: energy spectra of the dd fusion events measured in Run 8 and in Run 9

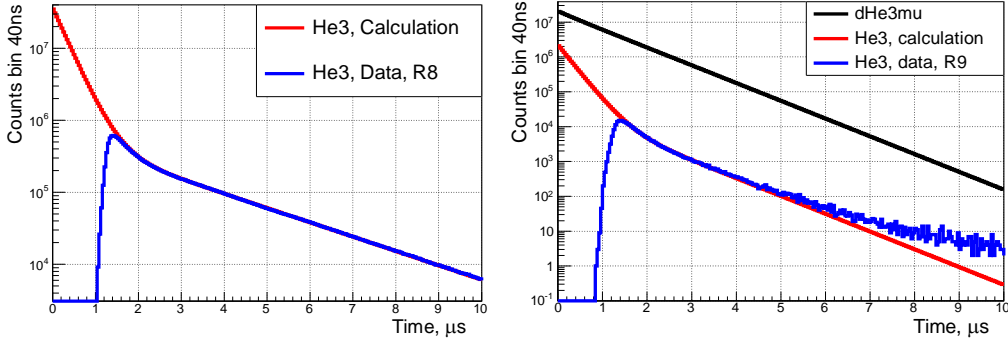


Fig. 4. Time distributions of the $dd \rightarrow {}^3\text{He} + n + \mu$ events in Run 8 (red line in the left panel) and in Run 9 (red line in the right panel) calculated according to the scheme in Fig. 3 with the kinetics parameters from [11]. Time distributions of the ${}^3\text{He}$ signals separated in time from the muon stop signals measured in Run 8 (blue line in the left panel) and in Run 9 (blue line in the right panel). The calculated time distribution of the ${}^3\text{He}d\mu$ molecules (black line in the right panel)

The largest peak in the energy spectrum of the dd fusion events shown in Fig. 3 is due to ${}^3\text{He}$ (0.82 MeV) from the $dd \rightarrow {}^3\text{He} + n + \mu$ fusion channel. The next peak is due to ${}^3\text{He}\mu$ (0.82 MeV) from the $dd \rightarrow {}^3\text{He}\mu + n$ fusion channel. Both peaks proved to be shifted from 0.82 MeV to lower energies because of the electron-ion recombination, the effect being larger for doubly charged ${}^3\text{He}^{++}$ ions than for singly charged ${}^3\text{He}\mu^+$ ions. The difference in the ${}^3\text{He}$ peak positions in Run 8 and in Run 9 is because the recombination effect is by 9% lower in the $D_2 + {}^3\text{He}$ (5%) gas mixture than in pure D_2 gas. The third peak is due to pileup of the ${}^3\text{He}$ signals with the ${}^3\text{He}$ or ${}^3\text{He}\mu$ signals from the next fusion cycle. The weights of the corresponding peaks in Fig. 3 are:

$$w({}^3\text{He}) / w({}^3\text{He}\mu) / w({}^3\text{He}{}^3\text{He}) = 0.842 / 0.125 / 0.033. \quad (8)$$

The fusion-in-flight probabilities for these types of events correlate as:

$$F({}^3\text{He}) / F({}^3\text{He}\mu) / F({}^3\text{He}{}^3\text{He}) = 1. / 2.3 / 2. \quad (9)$$

The probability $F({}^3\text{He}\mu)$ is larger than $F({}^3\text{He})$ proportionally to the length R of their tracks: $R({}^3\text{He}) = 0.28$ mm and $R({}^3\text{He}\mu) = 0.64$ mm.

In our analysis, we normalize the number of the fusion-in-flight events to the yield of ${}^3\text{He}$ (0.82 MeV) in the first peak in the spectrum shown in Fig. 3. Note that this yield is measured with the efficiency $\varepsilon({}^3\text{He}) = 0.95$ because of 5% losses in the tail below the low energy cut. The probability $F^*({}^3\text{He})$ to produce

a fusion-in-flight event per one ${}^3\text{He}$ (0.82 MeV) signal in the first peak in Fig. 3 is given by the following expression:

$$F^*({}^3\text{He}) = F({}^3\text{He}) \cdot [w({}^3\text{He}) + 2.3 \cdot w({}^3\text{He}\mu) + 2 \cdot w({}^3\text{He}{}^3\text{He})] / [w({}^3\text{He}) \cdot \varepsilon({}^3\text{He})] = 4.04 \cdot 10^{-5}, \quad (10)$$

where $F({}^3\text{He}) = 2.7 \cdot 10^{-5}$ is the probability to produce a fusion-in-flight event by a ${}^3\text{He}$ (0.82 MeV) particle stopping in the D_2 gas. This probability was calculated using the available ${}^3\text{He} + d$ fusion cross sections in the ${}^3\text{He}$ energy range below 1 MeV [12]. The precision of the calculated value of $F({}^3\text{He})$ is $\sim 5\%$.

The obtained value of $F^*({}^3\text{He})$ can be used to calculate the expected yield of the ${}^3\text{He} + d$ fusion-in-flight events from the measured number of the ${}^3\text{He}$ (0.82 MeV) signals. Figure 4 shows the results of such measurements in Run 8. One can see that after $t = 1.5 \mu\text{s}$ the measured ${}^3\text{He}$ distribution proved to be in excellent (without any renormalization) agreement with the distribution calculated on the basis of the kinematics scheme in Fig. 3. The drop below $t = 1.5 \mu\text{s}$ is related with overlapping of the ${}^3\text{He}$ signal with the muon stop signal. The averaged value $t^* = 1.28 \mu\text{s}$ can be considered as the minimal time between the ${}^3\text{He}$ signal and the muon signal needed for separation of these signals from each other. The total ${}^3\text{He}$ yield (the first peak in Fig. 4) in Run 8 was found to be $N({}^3\text{He}) = 1.283 \cdot 10^7$. Then, the expected yield of the ${}^3\text{He}d$ fusion-in-flight events in the time interval $t \geq 1.28 \mu\text{s}$ can be calculated as:

$$N({}^4\text{He} + p)_{\text{FinF}} = N({}^3\text{He}) F^*({}^3\text{He}) = 518. \quad (11)$$

Note that the minimal separation time $t^* = 1.28 \mu\text{s}$ should be practically the same for the d ${}^3\text{He}$ fusion-in-flight and for the ${}^3\text{He}d\mu$ fusion events. Therefore, we can use this value to calculate the number of the ${}^3\text{He}d\mu$ molecules produced in Run 9 in the time interval $t \geq 1.28 \mu\text{s}$. Similarly to Run 8, Fig. 4 presents the calculated and the measured time distributions of the $dd \rightarrow {}^3\text{He} + n + \mu$ events in Run 9. In addition, it presents the calculated time distribution of the produced ${}^3\text{He}d\mu$ molecules. From these data, we determine the registered number of the ${}^3\text{He}$ particles, $N({}^3\text{He}) = 3.34 \cdot 10^5$, and the number of the ${}^3\text{He}d\mu$ molecules produced at $t \geq 1.28 \mu\text{s}$, $N({}^3\text{He}d\mu) = 1.14 \cdot 10^8$.

The full data set from Run 8 and Run 9 was analysed with the goal to identify the ${}^4\text{He} + p$ events. The muon stops were selected to be inside the TPC fiducial volume (Fig. 2). Also, it was required that the muon stops were accompanied by the muon decay electrons registered in the eSC electron detector in the time window $0-25 \mu\text{s}$ after the muon stop. The number of thus selected muon stops is $\tilde{N}_\mu = 6.3 \cdot 10^9$ and $\tilde{N}_\mu = 1.0 \cdot 10^9$ for Run 8 and Run 9, respectively. Table 2 summarizes the statistics collected in Run 8 and Run 9 and presents the number of expected fusion-in-flight events calculated according to expression (10).

Table 2

The number of the selected muon stops \tilde{N}_μ ; the number of the registered ${}^3\text{He}$ signals $N({}^3\text{He})$ (the first peak in the energy spectra in Fig. 3); the number of the produced ${}^3\text{He}d\mu$ molecules $N({}^3\text{He}d\mu)$; and the number of the expected fusion-in-flight events $N_{\text{FinF}}(4\pi)$ in Run 8 and in Run 9 at $t \geq 1.28 \mu\text{s}$

Run	\tilde{N}_μ	$N({}^3\text{He})$	$N({}^3\text{He}d\mu)$	$N_{\text{FinF}}(4\pi)$ Expected for 4π geometry
Run 8	$6.3 \cdot 10^9$	$1.28 \cdot 10^7$	—	518 ± 26
Run 9	$1.0 \cdot 10^9$	$3.34 \cdot 10^5$	$1.14 \cdot 10^8$	14 ± 0.7

At the first step, the selection of the candidates for the ${}^4\text{He} + p$ events was done with the following criteria:

- there should be a signal at the muon stop pad P0 ($E_{\text{P0}} \geq 1.0 \text{ MeV}$) separated in time from the muon signal and accompanied by two signals at a sequence of two neighbour pads P1 and P2;
- the pulses on pads P0, P1, and P2 should overlap in time to form a continuous track;

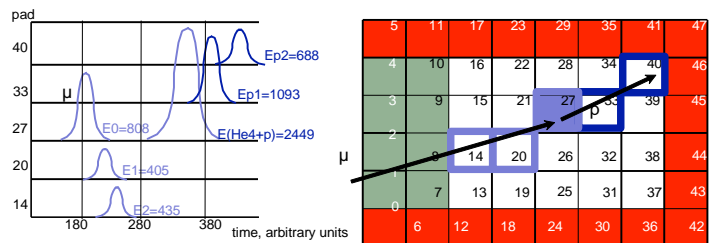


Fig. 5. Flash ADC display of a candidate for the ${}^4\text{He} + p$ event. It shows a muon trajectory with the muon stop on Pad 27 followed by the signals on Pad 27, Pad 33, and Pad 40. The pads included in the selected muon stop fiducial area are indicated with white colour

- there should be only one active P1 pad in between P0 and P2.

Figure 5 demonstrates an example of a registered candidate. The further selection of the candidates for the ${}^4\text{He} + p$ events was done using information on the energy deposits on pads P0, P1, and P2 taking into account the electron-ion recombination in the tracks.

The recombination effect reveals itself as a difference between the measured energy of the signal E_{meas} and the real energy of the particle E : $E_{\text{meas}} = E - E_{\text{recomb}}$ (see Fig. 6b). The value of E_{recomb} was determined using the measured signals from the alpha sources, ${}^{240}\text{Pu}$ ($E_{\alpha} = 5.156$ MeV) and ${}^{241}\text{Am}$ ($E_{\alpha} = 5.480$ MeV) and from the ${}^3\text{He}$ (0.82 MeV) peak using for interpolation the following expression:

$$E_{\text{recomb}} = E \left(A \cdot \sqrt{\Theta} + B \cdot \Theta \right), \text{ where } \Theta = Z^2 M/E. \quad (12)$$

Here Z and M are the charge and the mass of the ionizing particle. For Run 9, the fit parameters were found to be $A = (6.26 \pm 0.15) \cdot 10^{-3}$, $B = -(0.0095 \pm 0.0015) \cdot 10^{-3}$. In Run 8, the recombination effect is larger by a factor of 1.09. Figure 6a

shows the MC energy spectrum on pad P0 calculated for the ${}^3\text{He} + d \rightarrow {}^4\text{He} + p$ fusion-in-flight events in Run 8 taking into account the recombination effect and the TPC energy resolution. Also shown is the expected energy spectrum for the muon catalyzed d ${}^3\text{He}$ fusion events in Run 9. Figure 7a presents the energy spectrum on pad P0 of 455 ${}^4\text{He} + p$ candidates selected in Run 8 according to the above mentioned criteria in the region $E_{P0} \geq 0.85$ MeV.

The next step includes the analysis of the energy spectra on pads P1 and P2. The range of the 14 MeV protons in the TPC is $R_p = 23$ cm with $dE/dx = 0.35$ MeV/cm. The energy deposited by a proton in the zone of pads P1 and P2 should be around 0.5 MeV. Therefore, we use the region $E_{P1} \leq 1$ MeV, $E_{P2} \leq 1$ MeV for selection of the candidates for the ${}^4\text{He} + p$ events. This resulted in 182 events in Run 8 and 12 events in Run 9.

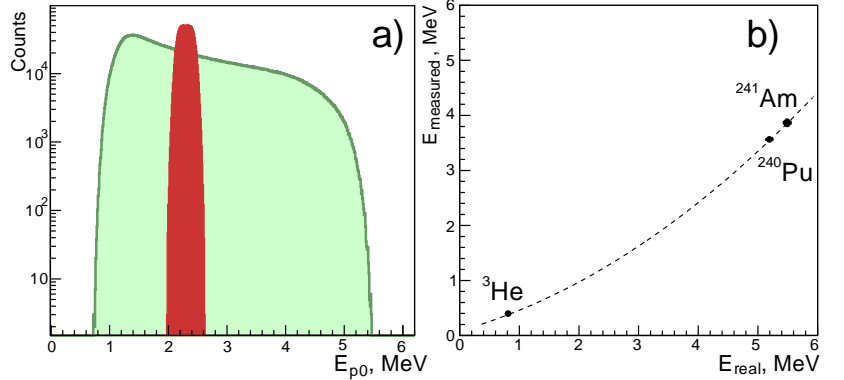


Fig. 6. a) MC energy spectra on pad P0 for the ${}^3\text{He} + d$ fusion-in-flight events in Run 8 (green colour) and for the muon catalyzed d ${}^3\text{He}$ fusion events in Run 9 (red colour). b) The measured energy versus the real energy of the ${}^4\text{He}$ particles in Run 9. The dashed line represents the results of calculations using expression (12) with the parameters $A = 6.26 \cdot 10^{-3}$ and $B = -0.0095 \cdot 10^{-3}$ determined from the fit to the measured ${}^{241}\text{Am}$ and ${}^{240}\text{Pu}$ alpha peak positions and to the ${}^3\text{He}$ (0.82 MeV) peak position

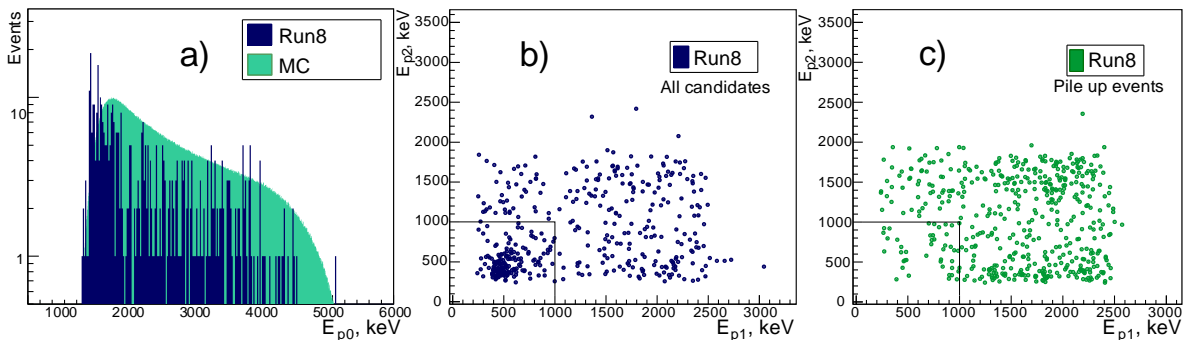
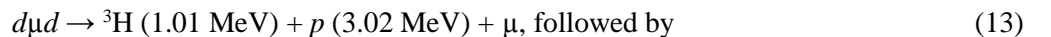


Fig. 7. a) Energy spectrum on pad P0 of the 455 ${}^4\text{He} + p$ candidates selected in Run 8; b) Energy distribution on pads P1 and P2 of the 455 ${}^4\text{He} + p$ candidates in Run 8; c) Energy distribution of the dd fusion pileup events on pads P1 and P2 (506 events)

However, besides the ${}^4\text{He} + p$ events, one can see in Fig. 7b some background with very special distribution ended sharply at $E_{P1} = 2.5$ MeV and at $E_{P2} = 1.8$ MeV. The nature of this background is understood. It is due to piling up of two successive $d\mu d$ fusion reactions:



$d\mu d \rightarrow {}^3\text{He} (0.82 \text{ MeV}) + n (2.45 \text{ MeV}) + \mu$, or vice versa.

Such events can produce signals on P0 (due to 1.1 MeV ${}^3\text{H}$ and 0.82 MeV ${}^3\text{He}$), on P1 (due to the 3.02 MeV proton with $R_p = 13 \text{ mm}$), and on P2 (due to scattering of the 2.45 MeV neutron on deuterons). The available in Run 8 experimental data allow to reproduce directly this background by collecting the events with signals on P0 and P1 accompanied by signals on the pads which are not joining the pads P0 and P1. Figure 7c presents the $E_{P1} \times E_{P2}$ plot of such events. To separate the ${}^4\text{He} + p$ events from the dd fusion pileup events, the number of events in the $E_{P1} \times E_{P2}$ plot (Fig. 7c) in the region $E_{P1} \geq 1 \text{ MeV}$, $E_{P2} \geq 1 \text{ MeV}$ was normalized to the number of events in the corresponding region in Fig. 7b, and the number of the dd fusion pileup events in the zone $E_{P1} \leq 1 \text{ MeV}$, $E_{P2} \leq 1 \text{ MeV}$ was determined: $N_{\text{pileup}}(\text{R8}) = 25$. Then the number of the registered $d {}^3\text{He}$ fusion-in-flight events was obtained: $N_{\text{FinF}}(\text{R8}) = 182 - 25 = 157$. Comparison of this number with the expected number of the ${}^3\text{He} + d$ fusion-in-flight events gives the registration efficiency of the fusion-in-flight events: $\varepsilon_{\text{FinF}} = (30 \pm 3)\%$. This value is valid also for the registration efficiency of the muon catalyzed $d {}^3\text{He}$ fusion. The quoted error is determined by the error in the number of the detected fusion-in-flight events and by the error in the calculated probability to produce a fusion-in-flight event by the 0.82 MeV ${}^3\text{He}$ particle in the D_2 gas.

The considered above two types of events constitute the main background in Run 9 aimed at observation of the muon catalyzed fusion reaction ${}^3\text{He}d \rightarrow {}^4\text{He} + p$. Based on the results obtained in Run 8, we can calculate the expected background in Run 9 using the following expressions :

$$\begin{aligned} N_{\text{FinF}}(\text{R9}) &= N_{\text{FinF}}(\text{R8}) \cdot N({}^3\text{He})_{\text{R9}} / N({}^3\text{He})_{\text{R8}} \cdot C_d(\text{R9})/C_d(\text{R8}), \\ N_{\text{pileup}}(\text{R9}) &= N_{\text{pileup}}(\text{R8}) \cdot N({}^3\text{He})_{\text{R9}} / N({}^3\text{He})_{\text{R8}} \cdot P_{\text{pileup}}(\text{R9}) / P_{\text{pileup}}(\text{R8}), \\ N_{\text{bgr}}(\text{R9}) &= N_{\text{FinF}}(\text{R9}) + N_{\text{pileup}}(\text{R9}), \end{aligned} \quad (14)$$

where the ratio of the registered ${}^3\text{He}$ signals $N({}^3\text{He})_{\text{R9}} / N({}^3\text{He})_{\text{R8}} = 0.026$; the ratio of the D_2 densities $C_d(\text{R9})/C_d(\text{R8}) = 0.95$; and the ratio of the dd fusion pileup probabilities $P_{\text{pileup}}(\text{R9})/P_{\text{pileup}}(\text{R8}) = 0.61$. The calculated in this way background predictions for Run 9 are as follows: $N_{\text{FinF}}(\text{R9}) = 3.87 \pm 0.3$, $N_{\text{pileup}}(\text{R9}) = 0.39 \pm 0.08$, $N_{\text{bgr}}(\text{R9}) = 4.3 \pm 0.4$. The quoted error in $N_{\text{bgr}}(\text{R9})$ is determined mostly by the statistical error in $N_{\text{FinF}}(\text{R8})$.

We can further reduce $N_{\text{bgr}}(\text{R9})$ by cutting the low energy part in the energy spectrum on pad P0 presented in Fig. 7a. The expected position of the signals from the muon catalyzed ${}^3\text{He}d \rightarrow {}^4\text{He} + p$ reaction is above $E_{P0} = 2.4 \text{ MeV}$ (Fig. 7a). Therefore, we can set the low energy cut at the energy up to $E_{P0} = 2.0 \text{ MeV}$ without noticeable decrease in the registration efficiency of the muon catalyzed ${}^3\text{He}d \rightarrow {}^4\text{He} + p$ reaction. Table 3 presents the background predicted for Run 9 for various E_{P0} cuts.

Another source of background in Run 9 might be the breakup reaction ${}^3\text{He}\mu \rightarrow d + n, p + 2n$. However, the energy deposit on pad P0 being rather small in such events, they could simulate the muon catalyzed ${}^3\text{He}d \rightarrow {}^4\text{He} + p$ fusion events only when piling up with the $dd \rightarrow {}^3\text{H} + p$ events. The calculated probability of such process is 0.5×10^{-7} per muon stop. In addition, it is suppressed by three orders of magnitude to a negligible level by requiring detection of the muon decay electron with the ePC/eSC detectors. Similarly, the muon capture on gas impurities (N_2) could be disregarded, especially taking into account very high purity (10^{-9}) of the D_2 gas in this experiment.

Table 3

Total number of selected ${}^4\text{He} + p$ candidates N_{tot} in Run 8 and in Run 9, the number of fusion-in-flight events N_{FinF} , and the number of dd fusion pile up events N_{pileup} registered in Run 8 and extrapolated to Run 9 for various cuts on the energy deposited on pad P0

EO cut	Run 8			Run 9	Run 9 background determined from Run 8		
	N_{tot}	N_{FinF}	N_{pileup}	N_{tot}	N_{FinF}	N_{pileup}	$N_{\text{bgr}} = N_{\text{FinF}} + N_{\text{pileup}}$
1.0 MeV	182	157	25	6	3.87 ± 0.31	0.39 ± 0.08	4.3 ± 0.4
1.6 MeV	117	93	24	3	2.30 ± 0.23	0.37 ± 0.08	2.7 ± 0.3
2.0 MeV	99	77	22	2	1.90 ± 0.22	0.34 ± 0.07	2.2 ± 0.3

Finally, two candidates for the muon catalyzed ${}^3\text{He}d$ fusion were registered with the predicted background of 2.2 ± 0.3 events.

Based on this observation, an upper confidence limit for the number of the muon catalyzed ${}^3\text{He}d$ fusion events was calculated by the method described in Refs. [13, 14] which takes into account the measured background uncertainty: $N_f \leq 3.1$ events at the 90% confidence level. This determines an upper limit for the effective muon catalyzed d ${}^3\text{He}$ fusion rate:

$$\lambda_f = N_f \cdot \lambda_{\text{dec}} / N_{3\text{Hed}\mu} \cdot \varepsilon_f \quad (15)$$

where $N_{3\text{Hed}\mu} = 1.14 \cdot 10^8$ is the number of the produced ${}^3\text{Hed}\mu$ molecules, $\lambda_{\text{dec}} = 7 \cdot 10^{11} \text{ s}^{-1}$ is the decay rate of the ${}^3\text{Hed}\mu$ molecule, $\varepsilon_f = 0.30$ is the detection efficiency of the ${}^3\text{He}d$ fusion events. This gives:

$$\lambda_f \leq 6.3 \cdot 10^4 \text{ s}^{-1} \text{ at 90\% C.L.} \quad (16)$$

4. Conclusion

An upper limit for the rate λ_f of muon catalyzed d ${}^3\text{He}$ fusion was set in this experiment performed with the $\text{D}_2 + {}^3\text{He}$ (5%) gas mixture at 31 K temperature with the gas density $\varphi = 6.5\%$ of the LHD:

$$\lambda_f \leq 6.3 \cdot 10^4 \text{ s}^{-1} \text{ at 90\% C.L.}$$

An important feature of this experiment was a possibility to determine the level of the background and the registration efficiency using data from the high statistical MuSun experiment performed with pure D_2 gas in the same experimental conditions.

The obtained limit for λ_f is close to that determined in our previous experiment [8] performed with the $\text{HD} + {}^3\text{He}$ (5.6%) gas mixture. On the other hand, it disagrees strongly with the rate $\lambda_f \approx 6 \cdot 10^5 \text{ s}^{-1}$ reported in [9] and thus rules out the statement made in [9] on observation of the muon catalyzed d ${}^3\text{He}$ fusion.

Based on the theoretical predictions [2–7], one could expect the rate $\lambda_f \approx 2.5 \cdot 10^4 \text{ s}^{-1}$, which would correspond to observation of 1.3 events in our experiment. Note that this experiment was performed as a supplement to MuSun with only one week running time. In a dedicated experiment with the same set-up, one could increase the sensitivity for detection of the muon catalyzed d ${}^3\text{He}$ fusion events by an order of magnitude due to several factors. This could be an experiment with the $\text{HD} + 5\% {}^3\text{He}$ gas mixture with some modifications of the TPC signals shaping and reduction of the dead time introduced by the “muon on request” system. In this case, the detection efficiency for the muon catalyzed d ${}^3\text{He}$ fusion events will be increased by a factor of five, while the fusion-in-flight background will be decreased by a factor of four. Therefore, assuming $\lambda_f \approx 2.5 \cdot 10^4 \text{ s}^{-1}$, one could register about 26 muon catalyzed d ${}^3\text{He}$ fusion events with 8 ± 1 background events in a four weeks running time experiment.

References

1. Y.A. Aristov *et al.*, *Yad. Phys.* **33**, 1066 (1981).
2. Y. Kino and M. Kamimura, *Hyperfine Interact.* **82**, 195 (1993).
3. A.V. Kravtsov *et al.*, *Z. Phys. D* **29**, 49 (1994).
4. S.S. Gershtein and V.V. Gusev, *Hyperfine Interact.* **82**, 205 (1993).
5. L.N. Bogdanova, V.I. Korobov and L.I. Ponomarev, *Hyperfine. Interact.* **118**, 187 (1999).
6. D.I. Abramov, V.V. Gusev and L.I. Ponomarev, *Hyperfine. Interact.* **119**, 127 (1999).
7. M.P. Faifman and L.I. Men'shikov, *Hyperfine Interact.* **119**, 127 (1999).
8. E.M. Maev *et al.*, *Hyperfine Interact.* **118**, 171 (1999).
9. V.M. Bystritsky *et al.*, *European Physical Journal D* **38**, 455 (2006).
10. V.A. Ganzha *et al.*, *PNPI Main Scientific Activities HEPD 2007–2012*, 106 (2013).
11. D.V. Balin, V.A. Ganzha, S.M. Kozlov *et al.*, *Phys. Part. Nuclei* **42**, 185 (2011);
D.V. Balin, V.A. Ganzha, S.M. Kozlov *et al.* *Particles and Nuclei* **42**, 361, Dubna (2011).
12. W.E. Kunz, *Phys. Rev.* **97**, 456 (1955); R.M. White, R.W.D. Resler, G.M. Hale,
Tech. Rep. IEAE NDS 177, International Atomic Energy Agency (1997).
13. T.M. Huber *et al.*, *Phys. Rev. D* **41**, 2709 (1990).
14. R.D. Cousins, V.L. Highland, *Nucl. Instr. and Meth. A* **320**, 331 (1992).